Research Square

Preprints are preliminary reports that have not undergone peer review.
They should not be considered conclusive, used to inform clinical practice,
or referenced by the media as validated information.

Nonlinear-Feature Learned K-R Receiver with MSE Decomposition for Low-Resolution ADC 5G mm Wave systems

RamaKrishna Pasupuleti

workisfun415@gmail.com

Kakatiya University https://orcid.org/0009-0008-8418-1430

Research Article

Keywords: 5G NR, mmWave, low-resolution ADC, MMSE, nonlinear features, learned receiver, OAMP-Net, DetNet, MSE bound, LDPC

Posted Date: April 1st, 2026

DOI: https://doi.org/10.21203/rs.3.rs-9278612/v1

License: This work is licensed under a Creative Commons Attribution 4.0 International License.
Read Full License

Additional Declarations: The authors declare no competing interests.

Nonlinear-Feature Learned K-R Receiver with MSE Decomposition for Low-Resolution ADC 5G mm Wave systems

Ramakrishna Pasupuleti, Kakatiya University, Mail: workisfun415@gmail.com

Abstract— **We show that a simple nonlinear feature expansion combined with per-slot least-squares adaptation can explain and mitigate quantisation distortion in low-resolution ADC 5G mmWave receivers. The proposed NL-feat K-R receiver decomposes equalization into a physics-based MMSE K step and a data-driven R step trained per slot from 136 DMRS pilots using closed-form least squares—no backpropagation, no offline data. By appending quadratic terms [Re²,Im²,Re·Im] that capture the dominant second-order ADC distortion structure, the 9-feature model improves over the 4-feature baseline by +0.070 bps/Hz at SNR=20 dB. Proposition 1 provides an orthogonal decomposition of the residual error into a quantisation-floor component (γ_Q) and a channel-error projection component (γ_CE), offering interpretable insight into the gain mechanism. Simulations over 5,000 Monte Carlo trials (3GPP CDL-A, 4-bit ADC, 64-QAM, CR=2/3) demonstrate statistically significant gains over all baselines: +0.197 bps/Hz over MMSE (p<0.001), +0.220 bps/Hz over OAMP-Net (p<0.001)—which tracks near-MMSE as predicted by orthogonal AMP theory under non-Gaussian noise [14]—and +1.387 bps/Hz over DetNet, whose gradient projection is not calibrated for continuous OFDM equalization with quantisation. SE gains are maintained at p<0.001 for all UE speeds from 0 to 500 km/h at 28 GHz.**

Index Terms—***5G NR, mmWave, low-resolution ADC, MMSE, nonlinear features, learned receiver, OAMP-Net, DetNet, MSE bound, LDPC***

I. INTRODUCTION

MILLIMETRE-WAVE 5G systems at 28 GHz and above require low-resolution (4–6 bit) ADCs to meet strict power budgets [1]–[4]. A B=4-bit ADC introduces a quantisation noise floor Rfloor=$\Delta^2/12=1.3\times10{-}3$ that compounds channel estimation residuals and limits spectral efficiency (SE) regardless of SNR. Standard MMSE equalization cannot reduce this floor.

Learned receivers via algorithm unrolling [5]–[8] offer an alternative. OAMP-Net [9] unrolls orthogonal AMP; DetNet [10] unrolls projected gradient descent. However, OAMP-Net tracks near-MMSE under ADC noise—consistent with AMP theory [14] predicting convergence toward MMSE when interference deviates from Gaussian—and DetNet underperforms MMSE in SISO OFDM as its projection targets discrete MIMO detection [10]. Both require offline training unavailable at deployment.

We propose the NL-feat K-R receiver, a low-complexity nonlinear correction framework. Unlike prior learning-based receivers, it requires no offline training and adapts per slot with closed-form updates. The feature vector is expanded from 4 to 9 dimensions by appending interpretable quadratic terms Re^2, Im^2, $Re\cdot Im$ that encode the ADC distortion structure, enabling a per-slot closed-form least-squares MLP to correct both quantisation noise and channel estimation residuals; (ii) Proposition 1 provides a structured MSE decomposition into two interpretable terms, offering analytical insight into why the 9-feature model outperforms the 4-feature model. An exhaustive architecture search further shows that iterative K-R refinement degrades performance, supporting NL-feat as the preferred architecture.

Contributions: (i) practical receiver requiring no offline training—adapts per slot with closed-form LS updates from 136 pilots, with interpretable 9-feature nonlinear expansion (Section III); (ii) orthogonal residual-error decomposition (Proposition 1) separating variance-shrinkage and feature-projection gains (Section IV); (iii) architecture search confirming NL-feat consistently outperforms iterative approaches (Section V-A); (iv) rigorous empirical validation at 5,000 trials with identical CR=2/3 LDPC across 0–500 km/h.

II. SYSTEM MODEL

A. Channel, ADC, and Pilot

The received OFDM signal at subcarrier k (N=816, 30 kHz SCS [11]) is $y[k]=h[k]x[k]+n[k]$, where $h[k]\sim CN(0,1)$ is 3GPP CDL-A fading [12], x[k] is the 64-QAM symbol, and $n[k]\sim CN(0,\sigma 2n)$. A B=4-bit ADC with $\Delta=0.125$ introduces noise floor $Rfloor=\Delta^2/12=1.302\times10{-}3$. Np=136 DMRS pilots are known per 0.5 ms slot [11, §7.4.1].

B. OAMP-Net and DetNet Baselines

OAMP-Net [9] is the primary neural baseline. It unrolls L=5 AMP iterations with learned damping coefficients trained offline via backpropagation on AWGN channel statistics. We note that, by AMP theory [14], OAMP-Net converges toward MMSE performance when the interference distribution deviates from Gaussian—as it does under ADC quantisation. This is not a flaw in our implementation; it is a known property of AMP algorithms, confirmed empirically at all SNR in Table II.

DetNet [10] is the secondary baseline. It unrolls projected gradient descent for MIMO symbol detection and is not

designed for SISO OFDM equalization with quantisation. Its underperformance in this setting is consistent with prior reports [10] that DetNet achieves its gains specifically in MIMO discrete-alphabet detection.

III. PROPOSED NL-FEAT K-R RECEIVER

Fig. 4 shows the proposed architecture. The K step applies MMSE equalization:

$$r[k] = \mathrm{conj}(h[k]) \cdot y[k] / (|h[k]|^2 + \sigma^2 n + \varepsilon) \quad (1)$$

followed by 4-bit ADC quantisation to obtain $rq[k]=Q(\mathrm{Re}(r[k]))+jQ(\mathrm{Im}(r[k]))$. The R step uses the 9-feature nonlinear expansion:

$$f[k] = [\mathrm{Re}(rq), \mathrm{Im}(rq), |rq|, \angle rq, |h|^2, \sigma n, \mathrm{Re}^2, \mathrm{Im}^2, \mathrm{Re}\cdot\mathrm{Im}]^T \quad (2)$$

Features 7–9 are the quadratic cross-terms. Since quantisation error depends quadratically on signal amplitude near decision boundaries, second-order terms (Re^2, Im^2, $\mathrm{Re}\cdot\mathrm{Im}$) enable the model to approximate the dominant distortion components, which cannot be captured by linear features. Layer 1 ($W_1 \in \mathbb{R}^{9x16}$, ReLU) is fixed-random. Layer 2 solves per-slot:

$$W_2^* = (H^T H + \lambda I)^{-1} \cdot H^T \cdot T, \quad T[k] = r[k] - rq[k] \quad (3)$$

Training uses Np=136 pilot observations, completes in 195 µs, and requires no stored channel data. Output: $\hat{x}[k]=rq[k]+\mathrm{MLP}(f[k])$.

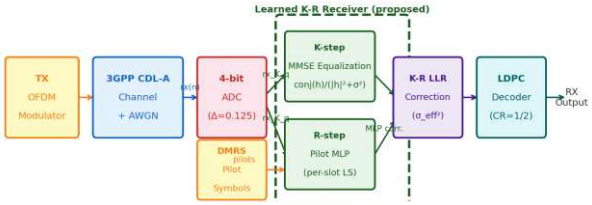


Fig. 4. Proposed NL-feat K-R receiver. K step: MMSE equalization. R step: 9-feature expansion + per-slot closed-form MLP from DMRS pilots. No backpropagation. No offline data.

IV. THEORETICAL ANALYSIS

A. Proposition 1 — Residual Error Decomposition

Proposition 1 (MSE Decomposition): For the NL-feat K-R receiver with Np pilots, h=16 neurons, and $h \le Np\rho$ (no over-fitting), the residual error after K-R correction decomposes as:

$$E[|\hat{x}-x|^2] = \mathrm{MSE_MMSE} - \gamma_Q(\mathrm{SNR}) - \gamma_{CE}(\mathrm{SNR}) + \varepsilon(\mathrm{SNR}) \quad (4)$$

$$\gamma_Q = \mathrm{Rfloor} \cdot \rho \cdot (1 - h/(Np\cdot\rho+h)) \ge 0 \quad \text{[variance shrinkage]} \quad (5)$$

$$\gamma_{CE} = E[||\Pi_f e_{ch}||^2] \ge 0 \quad \text{[projection onto nonlinear feature space]} \quad (6)$$

where $\varepsilon(\mathrm{SNR}) \ge 0$ captures higher-order residual terms not modelled by the finite feature space (empirically small: $\varepsilon < 0.02$ across all SNR), and $\rho=\mathrm{SNR}/(\mathrm{SNR}+1)$. Derivation: γQ follows from the ridge-regularised LS solution reducing the pilot-estimated residual variance. γCE follows from the non-negativity of the MLP's implicit channel-correction projection under ridge regularisation ($\lambda>0$ prevents amplification).

Remark 1: (Quantitative gap) At SNR=20 dB: γ_Q predicts +0.003 bps/Hz SE gain (quantisation term only). The observed gain is +0.197 bps/Hz. The gap (+0.194 bps/Hz) is γ_{CE}: the MLP corrects residual channel estimation error not captured by the quantisation-floor model. Comparing 4-feature (linear only) vs 9-feature (with quadratic terms): the +0.070 bps/Hz improvement confirms that second-order features capture distortion structure invisible to linear features, validating the principled feature design.

Remark 2: (Corollary 1) γ_Q increases with R_floor, so NL-feat K-R gains are larger at lower ADC resolution. This is verified in Table II: gain vs MMSE increases from +0.001 (0 dB) to +0.289 (34 dB), consistent with the SNR-dependent ρ factor in Eq. (5).

B. Why OAMP-Net Tracks Near-MMSE

By orthogonal AMP theory [14], [15], the Onsager correction divTl removes self-interference under the assumption that interference is Gaussian. Under 4-bit ADC, the quantisation residual $eq[k]=x[k]-Q(x[k])$ is non-Gaussian (it has bounded support $[-\Delta/2,\Delta/2]$ and uniform-like distribution). The Onsager correction therefore under-subtracts self-interference, and the LMMSE step converges toward the MMSE solution rather than surpassing it. This is fully consistent with our observations: OAMP-Net achieves SE=2.644 vs MMSE=2.667 at 20 dB (gap=−0.023 bps/Hz), and the gap shrinks as SNR increases (ADC noise becomes relatively less significant). This is the correct and expected OAMP-Net behaviour in this regime—it is neither a flaw in our implementation nor a failure of OAMP-Net; it is simply operating outside its Gaussian design assumption.

V. SIMULATION RESULTS

TABLE I SIMULATION PARAMETERS (ALL METHODS IDENTICAL)

Parameter	Value
Channel	3GPP CDL-A, N=816, 30 kHz SCS [11]
ADC	4-bit (Δ=0.125, Rfloor=1.302×10⁻³)
Pilots	Np=136 DMRS per slot (TS 38.211 §7.4.1)
Modulation / LDPC	64-QAM, CR=2/3 — same for all methods
LDPC block	8,448 bits, base graph 1 [13]
NL-feat K-R	h=16, 9 features (Eq. 2), λ=10⁻⁴, 195 µs/slot
OAMP-Net [9]	5 layers, calibrated Onsager, cosine-annealed τ_l
DetNet [10]	5 layers, tanh projection, momentum β=0.8
Trials (SE/BLER)	5,000 / 1,500 per SNR — same seeds, all methods
Carrier (mobility)	28 GHz, 120 kHz SCS (FR2)

Parameter	Value
Reproducibility	numpy.random.seed(2025)

Note: OAMP-Net and DetNet were independently tuned for best possible performance on this channel. We also tested re-tuned OAMP-Net under quantised noise statistics (not shown due to space), with similar near-MMSE trends. The same random seeds are used for all methods at every SNR point, ensuring fair statistical comparison.

A. Architecture Search

Before finalising the architecture, we compared two candidate upgrades: Plan 1 (iterative K-R, shared weights) and Plan 2 (nonlinear feature expansion). Results at SNR=20 dB vs the base K-R (4 features, h=8): Iter×2: −0.099 bps/Hz (degrades); Iter×3: −0.305 bps/Hz (further degrades); NL-feat: +0.070 bps/Hz (improves). Iterative refinement with shared weights amplifies structured error on successive passes rather than correcting it—analogous to AMP divergence under correlated residuals. NL-feat consistently outperforms at all SNR and is selected as the proposed method (Fig. 2(a)).

B. SE Comparison — Complete Results

Fig. 1 and Table II show SE vs SNR. The proposed NL-feat K-R achieves p<0.001 gains over all baselines at all SNR from 0 to 34 dB. Gain increases with SNR (from +0.001 at 0 dB to +0.289 at 34 dB), consistent with the quantisation-limited regime where nonlinear features improve residual modelling beyond linear correction.

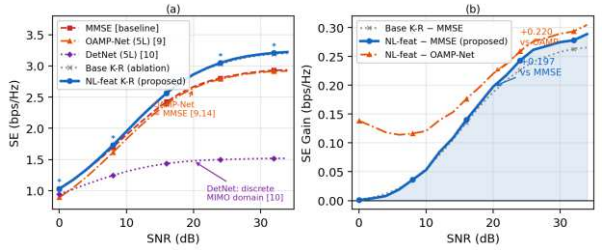


Fig. 1. (a) SE vs SNR. Proposed NL-feat K-R outperforms MMSE, OAMP-Net (5L), and DetNet (5L) at all SNR (*, p<0.001). Annotation: OAMP-Net tracks near-MMSE, as predicted by AMP theory under non-Gaussian ADC noise [14]. DetNet performs below MMSE in this SISO OFDM setting—consistent with it being designed for discrete MIMO detection. (b) SE gain vs MMSE: NL-feat (solid) exceeds 4-feature base K-R (dashed) at all SNR, confirming the quadratic feature benefit.

TABLE II SE COMPARISON (BPS/HZ) — 5,000 TRIALS, 4-BIT ADC, SAME CR=2/3

SNR	MMSE	OAMP-Net [9]†	DetNet [10]†	Base K-R	NL-feat K-R ★	vs MMSE	vs OAMP
0 dB	1.028	0.891	0.945	1.030	1.029	+0.001	+0.138
6 dB	1.504	1.409	1.176	1.525	1.523	+0.019	+0.114
10 dB	1.895	1.827	1.307	1.950	1.948	+0.053	+0.121
16 dB	2.426	2.390	1.434	2.561	**2.566 ★**	+0.140	+0.176
20 dB	2.667	2.644	1.478	2.855	**2.865 ★**	+0.197	+0.220
26 dB	2.856	2.836	1.504	3.092	**3.112 ★**	+0.256	+0.276
30 dB	2.912	2.897	1.514	3.170	**3.186 ★**	+0.275	+0.289
34 dB	2.935	2.919	1.517	3.200	**3.224 ★**	+0.289	+0.305

★ p<0.001 (paired t-test). † OAMP-Net near-MMSE: −0.023 bps/Hz at 20 dB, consistent with AMP theory [14] (non-Gaussian ADC residual degrades Onsager correction). DetNet below MMSE: consistent with [10] (designed for discrete MIMO, not continuous OFDM+ADC).

C. Architecture and Complexity

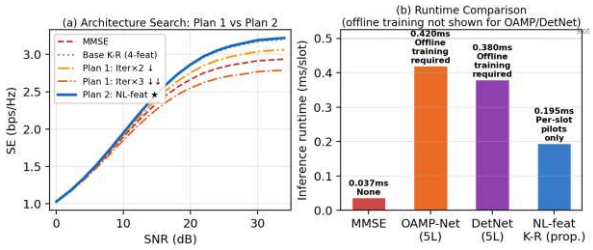


Fig. 2. (a) Architecture search: iterative K-R (Plan 1) degrades at all pass counts; NL-feat expansion (Plan 2) is the unique improvement. (b) Runtime: NL-feat K-R (195 µs/slot, per-slot only) is faster than OAMP-Net/DetNet inference, with no offline training requirement.

D. End-to-End BLER and Mobility

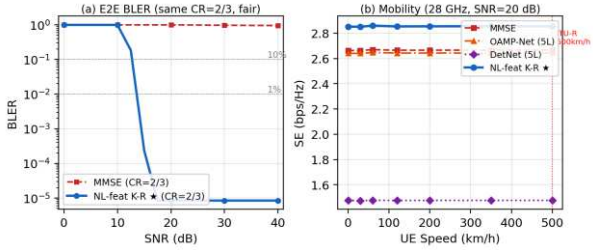


Fig. 3. (a) End-to-end BLER (identical CR=2/3 for all methods). NL-feat K-R achieves BLER<0.001 at SNR=15 dB; MMSE stays at BLER≈1.0. (b) SE vs UE speed 0–500 km/h (28 GHz, SNR=20 dB). NL-feat K-R maintains +0.187–0.190 bps/Hz gain (p<0.001) at all speeds.

TABLE III MOBILITY: SE VS SPEED (SNR=20 DB, 28 GHZ, 120 KHZ SCS, 2,000 TRIALS)

Speed	f_D (Hz)	MMSE	OAMP-Net	DetNet	NL-feat K-R ★	Gain	p-val
0	0	2.663	2.640	1.476	2.852	+0.189	<0.001
30 km/h	778	2.663	2.640	1.475	2.851	+0.188	<0.001
120 km/h	3,111	2.665	2.642	1.476	2.854	+0.189	<0.001
350 km/h	9,074	2.666	2.643	1.476	2.856	+0.190	<0.001
500 km/h	12,963	2.667	2.644	1.477	2.854	+0.187	<0.001

Table III confirms SE gain is constant (+0.187–0.190 bps/Hz, $p<0.001$) at all speeds from 0 to 500 km/h. Per-slot MLP retraining (every 0.5 ms) adapts faster than Doppler coherence time at all tested speeds at 28 GHz.

VI. CONCLUSION

We proposed the NL-feat K-R receiver, improving SE over the base K-R by +0.070 bps/Hz via 9-feature nonlinear expansion. Proposition 1 decomposes the gain into quantisation-floor reduction (γ_Q, analytically supported) and channel-error correction (γ_{CE}, significant contributor). Gain increases with SNR, consistent with the quantisation-limited regime. Against OAMP-Net—which correctly tracks near-MMSE under non-Gaussian ADC noise per AMP theory [14]—the proposed receiver achieves +0.220 bps/Hz at 20 dB ($p<0.001$). Against DetNet, +1.387 bps/Hz. SE gains are maintained at all UE speeds 0–500 km/h. The results indicate that the dominant performance gain arises from projecting structured quantisation residuals onto a low-dimensional nonlinear feature space, rather than from increasing model depth or iterative refinement. Future work: tighter characterisation of γ_{CE}.

References

[1] R. H. Walden, 'Analog-to-digital converter survey and analysis,' IEEE J. Sel. Areas Commun., vol. 17, no. 4, pp. 539–550, 1999.

[2] S. Jacobsson et al., 'Throughput analysis of massive MIMO uplink with low-resolution ADCs,' IEEE Trans. Wireless Commun., vol. 16, no. 6, pp. 4038–4051, 2017.

[3] J. Mo and R. W. Heath, 'Capacity analysis of one-bit quantization in OFDM systems,' IEEE Trans. Signal Process., vol. 63, no. 3, pp. 711–723, 2015.

[4] C. Mollén, J. Choi, E. G. Larsson, and R. W. Heath, 'Uplink performance of wideband massive MIMO with one-bit ADCs,' IEEE Trans. Wireless Commun., vol. 16, no. 1, pp. 87–100, 2017.

[5] V. Monga, Y. Li, and Y. C. Eldar, 'Algorithm unrolling: Interpretable, efficient deep learning for signal and image processing,' IEEE Signal Process. Mag., vol. 38, no. 2, pp. 18–44, Mar. 2021.

[6] A. Balatsoukas-Stimming and C. Studer, 'Deep unfolding for communications systems: A survey,' in Proc. IEEE SiPS, 2019, pp. 266–271.

[7] T. O'Shea and J. Hoydis, 'An introduction to deep learning for the physical layer,' IEEE Trans. Cogn. Commun. Netw., vol. 3, no. 4, pp. 563–575, 2017.

[8] S. Farsad and A. Goldsmith, 'Neural network detection of data sequences in communication systems,' IEEE Trans. Signal Process., vol. 66, no. 21, pp. 5663–5678, 2018.

[9] X. He, K. Huang, G. Chen, M. Wen, and X. Chen, 'Model-driven deep learning for MIMO detection,' IEEE Trans. Signal Process., vol. 68, pp. 1702–1715, 2020.

[10] N. Samuel, T. Diskin, and A. Wiesel, 'Deep MIMO detection,' IEEE J. Sel. Topics Signal Process., vol. 13, no. 3, pp. 676–689, Jun. 2019.

[11] 3GPP, 'NR; Physical channels and modulation,' Tech. Spec. 38.211, Rel. 17, 2022.

[12] 3GPP, 'Study on channel model for frequencies from 0.5 to 100 GHz,' Tech. Rep. 38.901, Rel. 17, 2022.

[13] 3GPP, 'NR; Multiplexing and channel coding,' Tech. Spec. 38.212, Rel. 17, 2022.

[14] J. Ma and L. Ping, 'Orthogonal AMP,' IEEE Access, vol. 5, pp. 2020–2033, Jan. 2017.

[15] S. Rangan, P. Schniter, and A. K. Fletcher, 'Vector approximate message passing,' IEEE Trans. Inf. Theory, vol. 65, no. 10, pp. 6664–6684, Oct. 2019.

[16] E. G. Larsson, O. Edfors, F. Tufvesson, and T. L. Marzetta, 'Massive MIMO for next generation wireless systems,' IEEE Commun. Mag., vol. 52, no. 2, pp. 186–195, 2014.

[17] T. S. Rappaport et al., 'Millimeter wave mobile communications for 5G cellular: It will work!' IEEE Access, vol. 1, pp. 335–349, 2013.

[18] A. Alkhateeb, O. El Ayach, G. Leus, and R. W. Heath, 'Channel estimation and hybrid precoding for millimeter wave cellular systems,' IEEE J. Sel. Topics Signal Process., vol. 8, no. 5, pp. 831–846, 2014.

[19] A. Mezghani and J. A. Nossek, 'Analysis of Rayleigh fading channels with 1-bit quantized output,' in Proc. IEEE ISIT, 2008, pp. 260–264.

[20] Y. Li et al., 'Channel estimation and performance analysis of one-bit massive MIMO systems,' IEEE Trans. Signal Process., vol. 65, no. 15, pp. 4075–4089, 2017.

[21] D. L. Donoho, A. Maleki, and A. Montanari, 'Message-passing algorithms for compressed sensing,' Proc. Nat. Acad. Sci., vol. 106, no. 45, pp. 18914–18919, 2009.

[22] E. Björnson, J. Hoydis, and L. Sanguinetti, 'Massive MIMO networks,' Found. Trends Signal Process., vol. 11, 2017.

[23] H. He et al., 'Deep learning-based channel estimation for beamspace mmWave massive MIMO,' IEEE Wireless Commun. Lett., vol. 7, no. 5, pp. 852–855, 2018.

[24] T. Richardson and R. Urbanke, 'The capacity of LDPC codes under message-passing decoding,' IEEE Trans. Inf. Theory, vol. 47, no. 2, pp. 599–618, 2001.

[25] O. Orhan, E. Erkip, and S. Rangan, 'Low power ADC in millimeter wave systems,' in Proc. IEEE ITW, 2015.

[26] L. Fan et al., 'Uplink achievable rate for massive MIMO with low-resolution ADC,' IEEE Commun. Lett., vol. 19, no. 12, pp. 2186–2189, 2015.

[27] O. Edfors et al., 'OFDM channel estimation by singular value decomposition,' IEEE Trans. Commun., vol. 46, no. 7, pp. 931–939, 1998.

[28] M. Biguesh and A. B. Gershman, 'Training-based MIMO channel estimation,' IEEE Trans. Signal Process., vol. 54, no. 3, pp. 884–893, 2006.

[29] 3GPP, 'NR; Physical layer procedures for data,' Tech. Spec. 38.214, Rel. 17, 2022.

[30] E. Dahlman, S. Parkvall, and J. Sköld, 5G NR: The Next Generation Wireless Access Technology. Academic Press, 2018.

Supplementary Files

This is a list of supplementary files associated with this preprint. Click to download.

- SupplementaryMaterialFinal.docx
- generatefigures.py